Mineralogical Magazine (2023), **87**, 659–669
doi:10.1180/mgm.2023.49

CAMBRIDGE UNIVERSITY PRESS

Article

Occurrence and crystal chemistry of austinite, conichalcite and zincolivenite from the Peloritani Mountains, northeastern Sicily, Italy

Daniela Mauro[1,2], Cristian Biagioni[2], Jiří Sejkora[3] and Zdeněk Dolníček[3]

[1]Museo di Storia Naturale, Università di Pisa, Via Roma 79, 56011 Calci (PI), Italy; [2]Dipartimento di Scienze della Terra, Università di Pisa, Via Santa Maria 53, 56126 Pisa, Italy; and [3]Department of Mineralogy and Petrology, National Museum, Cirkusová 1740, 193 00, Praha 9, Czech Republic

Abstract

A new occurrence of austinite, $CaZnAsO_4(OH)$, conichalcite, $CaCuAsO_4(OH)$, and zincolivenite, $CuZnAsO_4(OH)$, is described from the Tripi mine, Peloritani Mountains, Sicily, Italy. These species have been observed in euhedral crystals in vugs of a calcite vein and were characterised using single-crystal X-ray diffraction, electron microprobe analysis and micro-Raman spectroscopy. Austinite and conichalcite have isotypic relations, both crystallising in space group $P2_12_12_1$. Unit-cell parameters of austinite are $a = 7.4931(5)$, $b = 9.0256(6)$, $c = 5.9155(4)$ Å, $V = 400.06(5)$ Å^3; its crystal structure was refined on the basis of 1210 unique reflections with $F_o > 4\sigma(F_o)$ and 77 least-square parameters to $R_1 = 0.0236$. Conichalcite has unit-cell parameters $a = 7.419(10)$, $b = 9.111(11)$, $c = 5.867(7)$ Å and $V = 396.6(1.4)$ Å^3; the diffraction quality of its available grains was not good enough to allow a high-quality structural refinement. Chemical formulae of austinite and conichalcite are $Ca_{1.04(1)}Zn_{0.86(4)}Cu_{0.09(4)}As_{0.98(2)}P_{0.02(1)}O_4(OH)_{0.98}$ and $Ca_{0.98(1)}Fe^{2+}_{0.02(4)}Cu_{0.69(10)}Zn_{0.30(6)}As_{0.97(2)}P_{0.03(1)}O_4(OH)_{0.98}$, respectively. The new chemical data on the austinite–conichalcite isotypic pair, coupled with previous analyses, supports a possible miscibility gap between the compositions ($Zn_{0.25}Cu_{0.75}$) and ($Zn_{0.50}Cu_{0.50}$). Zincolivenite has unit-cell parameters $a = 8.4594(9)$, $b = 8.5324(8)$, $c = 5.9893(6)$ Å, $V = 432.30(12)$ Å^3 and space group *Pnnm*; its crystal structure was refined to $R_1 = 0.0230$ for 523 unique reflections with $F_o > 4\sigma(F_o)$ and 47 least-square parameters. Its chemical composition is $Cu_{0.73(5)}Zn_{1.25(5)}As_{1.01(1)}O_4(OH)_{1.01}$. The refinement of the crystal structure supports the ordering of Cu and Zn in two different crystallographic sites. Micro-Raman spectra of austinite, conichalcite and zincolivenite are discussed, with a focus on the O–H stretching region where local Zn and Cu arrangements affect the position of Raman bands in zincolivenite. These arsenates probably play an environmental role in the Peloritani area, where the occurrence of high contents of some potentially toxic elements in soils and stream sediments has been reported.

Keywords: austinite; conichalcite; zincolivenite; arsenate; crystal structure; Raman spectroscopy; Peloritani Mts; Sicily; Italy

(Received 22 May 2023; accepted 18 June 2023; Accepted Manuscript published online: 3 July 2023; Associate Editor: Peter Leverett)

Introduction

Arsenic ($Z = 33$) is considered one of the most worrying of the potential toxic elements (PTE), considering its prevalence, toxicity and potential for human exposure (e.g. Mitchell, 2014). Its possible dispersion in the environment and, ultimately, its bioavailability can be related to weathering processes affecting ore deposits, where As is widespread in several primary minerals (e.g. As-bearing pyrite, arsenopyrite and As-bearing sulfosalts). However, in order to understand its potential mobility, the occurrence of several attenuation processes, mainly related to the precipitation of As-minerals (both in oxidising or reducing environments) and the adsorption onto some minerals (e.g. Fe oxy-hydroxides) (e.g. Gieré *et al.*, 2003; Drahota and Filippi, 2009; Craw and Bowell, 2014), has to be taken into account. For these reasons, the mineralogical investigation of arsenate-bearing assemblages is crucial in assessing the fate of As in the environment.

Several researchers have pointed out the occurrence of high contents of some PTE, including As, in an area of the Peloritani Mountains (northeastern Sicily, Italy) where several small base-metal ore deposits are known (e.g. Saccà *et al.*, 2015 and references therein). For instance, De Vivo *et al.* (1993) stressed the presence of anomalous contents of As, Hg, Sb, Zn and Pb in stream sediments from this area, whereas Dongarrà *et al.* (2009) found high As concentrations in waters from mineralised areas. A geogenic source for the As contamination detected in the Peloritani Mountains was also suggested by Cangemi *et al.* (2021), agreeing with previous results of Cosenza *et al.* (2015) who reported high PTE content in soils from Fiumedinisi, Budali and Alì, related to the weathering of ore deposits and mine wastes.

In this respect, a better knowledge of the mineralogy of these deposits is mandatory. Among primary minerals, arsenopyrite and gersdorffite are known to occur (Donati *et al.*, 1978; Triscari and Saccà, 1982; Triscari, 1985; Mauro *et al.*, 2021) and minor As occurs in Pb/Sb sulfosalts (e.g. Triscari and Saccà,

Corresponding author: Daniela Mauro; Email: daniela.mauro@unipi.it
Cite this article: Mauro D., Biagioni C., Sejkora J. and Dolníček Z. (2023) Occurrence and crystal chemistry of austinite, conichalcite and zincolivenite from the Peloritani Mountains, northeastern Sicily, Italy. *Mineralogical Magazine* **87**, 659–669. https://doi.org/10.1180/mgm.2023.49

1984) and tetrahedrite-group minerals (Mauro *et al.*, 2021). The alteration of these species gives rise to the occurrence of supergene arsenates. La Valle (1898) reported the identification of annabergite, erythrite and possibly symplesite. Scorodite was described by Triscari and Saccà (1982). However, crystal chemical data for these arsenates are lacking and no further details on supergene assemblages was given. Recently, Mauro *et al.* (2022) investigated a supergene mineral belonging to the alunite supergroup from the Tripi mine (Alì, Messina Province), identifying it as the lead-iron phosphate kintoreite. The Tripi mine (latitude 38°00′50″N; 15°24′27″E), located some hundred metres SSW of the small hamlet of Alì, exploited a stratabound fine-banded ore, mainly composed of sphalerite and Ag-bearing galena, with rare pyrite and trace amounts of chalcopyrite, arsenopyrite, pyrrhotite and covellite; quartz and fluorite are gangue minerals (Saccà *et al.*, 2007). Supergene products are smithsonite, gypsum, hydrozincite, 'limonite' and malachite (Saccà *et al.*, 2007). Additional investigations of a suite of specimens sampled by one of us (DM) in the dumps of this abandoned mine allowed the identification of an interesting association of three distinct Zn-bearing arsenates, i.e. austinite, conichalcite and zincolivenite. To the best of our knowledge, these species have not been reported previously from the Sicilian ore deposits and, as regards austinite, this is the first Italian occurrence.

The aim of this paper is the crystal chemical characterisation of these three arsenates, improving the available crystallographic and spectroscopic data for these species.

Experimental

Specimen studied

The specimen studied is composed of a calcite vein with deeply oxidised pyrite crystals; in small vugs of the calcite vein, colourless to bright-green crystals can be observed (Fig. 1). Three distinct kinds of crystals were identified: Type 1, colourless bladed crystals, forming aggregates of transparent, sub-adamantine individuals, up to 1 mm in length; Type 2, bright green tabular crystals, with a vitreous lustre, up to 1 mm in size; and Type 3, pale green prismatic crystals, up to 0.2 mm, with a sub-vitreous lustre.

Chemical, spectroscopic and structural data on these three different crystal types were collected and allowed the identification of austinite (Type 1), conichalcite (Type 2) and zincolivenite (Type 3), respectively (see below).

Chemical analysis

Quantitative chemical analyses were performed at the National Museum of Prague (Czech Republic) using a Cameca SX 100 electron microprobe using the following analytical conditions: wavelength dispersive spectroscopy mode, accelerating voltage of 15 kV, beam current = 8 nA and beam size = 5 μm. The following standards (element, emission line) were used: albite (Na*K*α), baryte (Ba*L*α), Bi (Bi*M*α), celestine (S*K*α and Sr*L*β), chalcopyrite (Cu*K*α), clinoclase (As*L*α), Co (Co*K*α), diopside (Mg*K*α), fluorapatite (Ca*K*α and P*K*α), halite (Cl*K*α) hematite (Fe*K*α), LiF (F*K*α), rhodonite (Mn*K*α), sanidine (Al*K*α, K*K*α and Si*K*α), vanadinite (Pb*M*α and V*K*α) and ZnO (Zn*K*α). Contents of the above-listed elements not included in Table 1 were analysed quantitatively, but were consistently below the detection limit (ca. 0.03–0.08 wt.% for individual elements). Peak counting times (CT) were 20 s; CT for each background was one-half of the peak time. Matrix correction by *PAP* software (Pouchou and Pichoir, 1985) was applied to the data. Results of the electron microprobe analysis of the studied grains are given in Table 1.

Micro-Raman spectroscopy

Micro-Raman spectra of the minerals studied were collected using a Horiba Jobin-Yvon XploRA Plus apparatus, equipped with a motorised *x*–*y* stage and an Olympus BX41 microscope with a 50× objective (Dipartimento di Scienze della Terra, Università di Pisa). Raman spectra were excited using a 532 nm line of a solid-state laser, attenuated to 25% (i.e. 6.25 mW) in order to avoid any potential sample damage. The minimum lateral and depth resolution was set to a few μm. The system was calibrated using the 520.6 cm^{-1} Raman band of silicon before each experimental session. Spectra were collected through multiple acquisitions (3) with variable counting times, ranging from 30 to 180 s. Back-scattered radiation was analysed with a 1200 gr/mm grating monochromator. Experimental precision can be estimated at ± 2 cm^{-1}. Whenever necessary, Raman spectra were processed using *Fityk* (Wojdyr, 2010), subtracting the background and fitting the spectra to theoretical peak shapes using pseudo-Voigt functions.

X-ray crystallography

Single-crystal X-ray diffraction data were collected for austinite, conichalcite and zincolivenite using a Bruker D8 Venture diffractometer (50 kV and 1.4 mA) equipped with an air-cooled Photon III detector and microfocus Mo*K*α radiation (Centro per l'Integrazione della Strumentazione scientifica dell'Università di Pisa, Università di Pisa, Italy). For all the three crystals studied, the detector-to-crystal distance was set to 38 mm. The diffraction quality was good enough for crystals of austinite and zincolivenite, whereas no grains of conichalcite suitable for high-quality intensity data collection were found.

Data were collected using φ and ω scan modes, in 0.5° slices. Intensity data were integrated and corrected for Lorentz, polarisation, background effects and absorption using the *APEX4* (Bruker AXS Inc., 2022) software package. Crystal structure refinements were performed using *Shelxl–2018* (Sheldrick, 2015) and neutral scattering curves were taken from the *International Tables for Crystallography* (Wilson, 1992). Details of data collections and structure refinements are given in Table 2. Atomic coordinates and equivalent isotropic or isotropic displacement parameters are shown in Table 3, whereas selected bond distances are reported in Table 4. Bond-valence sums, calculated using the bond parameters of Gagné and Hawthorne (2015), are given in Table 5. Crystallographic information files of austinite and zincolivenite have been deposited with the Principal Editor of *Mineralogical Magazine* and are available as Supplementary material (see below). In the following, details of the structure refinements are briefly reported.

Austinite

A total of 1621 frames was collected, with exposure time of 10 s per frame. Unit-cell parameters are $a = 7.4931(5)$, $b = 9.0256(6)$, $c = 5.9155(4)$ Å, $V = 400.06(5)$ $Å^3$, space group $P2_12_12_1$, in agreement with systematic absences and the $|E^2-1|$ value (i.e. 0.684). The crystal structure was refined starting from the atomic coordinates given by Giuseppetti and Tadini (1988) for austinite. The

https://doi.org/10.1180/mgm.2023.49 Published online by Cambridge University Press

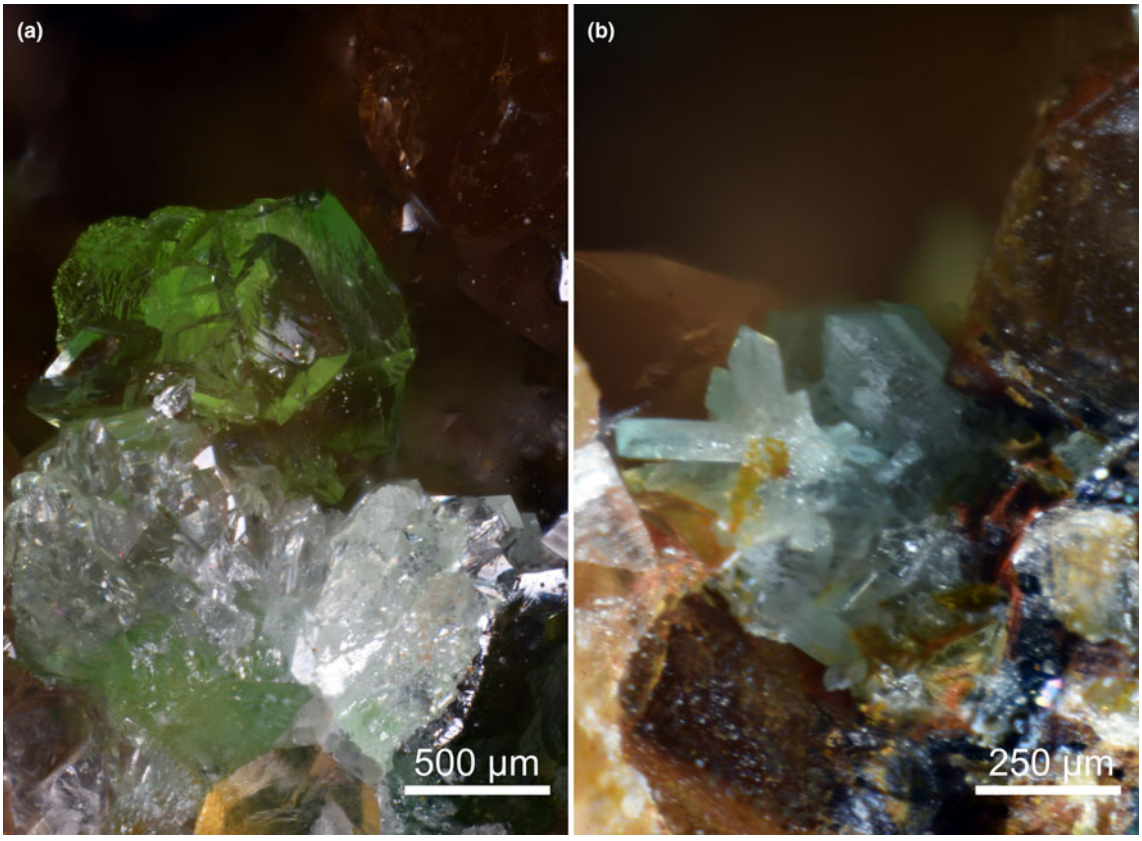

Figure 1. Arsenate minerals from the Tripi mine. (a) Colourless prismatic crystals of austinite associated with green conichalcite. (b) Prismatic crystals of zincolivenite. Specimens in private collection.

following scattering curves were used: Ca at the *Ca* site, As at the *As* site, O at the O(1)–O(5) sites, and H at the *H* site. Taking into account the similarity in the scattering factors of Cu ($Z = 29$) and Zn ($Z = 30$), and the results of electron microprobe analysis, showing a Zn/(Zn + Cu) atomic ratio of 0.90(4), only the scattering factor of Zn was used to model the site scattering of the *M* site. After several cycles of isotropic refinement, the R_1 factor converged to 0.0336, thus confirming the correctness of the structural model. A restraint on the O(5)–H bond distance was added and the displacement parameter of H was refined assuming it is 1.5 times that of U_{eq} of O(5). Racemic twinning was modelled, converging to a Flack parameter (Flack, 1983) of 0.17(2). After the introduction of the anisotropic displacement parameters for all atoms (but H), the R_1 decreased to 0.0236 for 1210 unique reflections with $F_o > 4\sigma(F_o)$ and 77 least-square parameters.

Conichalcite

Several grains of conichalcite were checked and all of them were polycrystalline, showing powder-like diffraction patterns. However, using a 30 × 30 × 30 µm grain, the refinement of the

Table 1. Electron microprobe data for arsenates from the Tripi mine.

	Austinite (*n* = 28)			Conichalcite (*n* = 9)			Zincolivenite (*n* = 22)		
Oxide	Wt.%	Range	σ	Wt.%	range	σ	Wt.%	range	σ
SO_3	0.01	0.00–0.16	0.04	0.03	0.00–0.12	0.05	–	–	–
P_2O_5	0.51	0.12–0.93	0.17	0.80	0.72–0.89	0.05	0.11	0.00–0.22	0.06
As_2O_5	42.59	41.30–43.49	0.55	41.31	39.77–42.41	0.77	40.05	39.57–41.12	0.44
SiO_2	0.02	0.00–0.26	0.07	0.03	0.00–0.28	0.09	0.04	0.00–0.33	0.11
Al_2O_3	0.00	0.00–0.09	0.02	0.08	0.00–0.39	0.12	0.03	0.00–0.26	0.08
MgO	0.05	0.00–0.63	0.13	–	–	–	–	–	–
CaO	21.78	21.20–22.27	0.27	20.37	19.85–20.80	0.31	0.01	0.00–0.06	0.02
MnO	0.00	0.00–0.06	0.01	0.05	0.00–0.42	0.14	0.01	0.00–0.08	0.03
FeO	–	–	–	0.47	0.00–3.04	0.97	–	–	–
CuO	2.79	0.76–6.86	1.15	20.22	14.81–23.15	3.02	20.18	17.80–22.61	1.48
ZnO	26.37	23.01–28.00	1.17	9.06	7.25–11.97	1.90	35.32	32.58–38.12	1.59
H_2O_{calc}*	3.32			3.26			3.06		
Total	97.44			95.68			98.81		

n = number of spot analyses. *Calculated in agreement with stoichiometry. σ = estimated standard deviation; – = not detected

https://doi.org/10.1180/mgm.2023.49 Published online by Cambridge University Press

Table 2. Summary of crystal data and parameters describing data collections and refinements for austinite and zincolivenite from the Tripi mine.

	Austinite	Zincolivenite
Crystal data		
Crystal size (mm)	0.120 × 0.095 × 0.065	0.070 × 0.050 × 0.040
Cell setting, space group	Orthorhombic, $P2_12_12_1$	Orthorhombic, *Pnnm*
a (Å)	7.4931(5)	8.4594(9)
b (Å)	9.0256(6)	8.5324(8)
c (Å)	5.9155(4)	5.9893(6)
V (Å^3)	400.06(5)	432.30(8)
Z	4	4
Data collection		
Radiation, wavelength (Å)	Mo*K*α, λ = 0.71073	Mo*K*α, λ = 0.71073
Temperature (K)	293(2)	293(2)
Maximum observed 2θ (°)	61.08	56.73
Measured reflections	9990	4860
Unique reflections	1232	586
Reflections $F_o > 4\sigma(F_o)$	1210	523
R_{int} after absorption correction	0.0492	0.0393
*R*σ	0.0307	0.0260
Range of *h*, *k*, *l*	$-10 \le h \le 10$ $-12 \le k \le 12$ $-8 \le l \le 8$	$-11 \le h \le 10$ $-11 \le k \le 11$ $-7 \le l \le 7$
Refinement		
R [F_o>4 σ F_o]	0.0236	0.0230
R (all data)	0.0243	0.0273
wR (on F_o^2)[1,2]	0.0604	0.0497
Goodness of fit	1.200	1.184
Flack parameter	0.17(2)	-
Number of least-squares parameters	77	47
Maximum and minimum residual peak (e^-/Å^3)	1.18 [at 1.34 Å from O(1)] −1.35 [at 0.51 Å from *M*]	0.94 [at 1.29 Å from *As*(1)] −1.08 [at 1.65 Å from H]

[1]Austinite: $w = 1/[\sigma^2(F_o^2)+(0.0263P)^2+0.7514P]$, where $P = (F_o^2+2F_c^2)/3$
[2]Zincolivenite: $w = 1/[\sigma^2(F_o^2)+2.3444P]$, where $P = (F_o^2+2F_c^2)/3$

unit-cell parameters of one of the individuals forming the polycrystalline aggregate was possible, selecting the sharp spots superimposed on diffraction rings. On the basis of 176 reflections in the 2θ range between 7.08 and 39.37°, the following unit-cell parameters were refined: $a = 7.419(10)$, $b = 9.111(11)$, $c = 5.867(7)$ Å and $V = 396.6(1.4)$ Å^3. Unfortunately, the intensity data had a very high R_{int} value (0.238), and the crystal structure refinement converged to a high R_1 value of 0.1101 for 342 reflections with $F_o > 4\sigma(F_o)$ and 49 least-square parameters (0.2334 for all the 871 measured reflections). For this reason, structural data of conichalcite are not discussed, and only electron microprobe data are presented.

Table 3. Sites, site occupancy factors*, fractional atom coordinates and isotropic (**) or equivalent isotropic displacement parameters (Å^2) for austinite and zincolivenite from the Tripi mine.

Site	*x*/*a*	*y*/*b*	*z*/*c*	$U_{iso/eq}$
Austinite				
Ca	0.36855(11)	0.67173(9)	0.52309(15)	0.00727(16)
M *	0.76363(7)	0.50626(7)	0.75690(10)	0.00977(14)
As	0.37763(5)	0.32282(4)	0.48323(7)	0.00454(12)
O(1)	0.5528(4)	0.4408(3)	0.5093(6)	0.0076(5)
O(2)	0.2091(5)	0.4369(4)	0.4117(6)	0.0102(6)
O(3)	0.6494(4)	0.7321(3)	0.7693(5)	0.0077(6)
O(4)	0.6030(4)	0.7093(3)	0.2408(5)	0.0085(5)
O(5)	0.8918(4)	0.5734(3)	0.4918(5)	0.0057(5)
H	0.989(6)	0.527(6)	0.471(11)	0.009**
Zincolivenite				
As(1)	0.24811(7)	0.23899(6)	½	0.00861(14)
Zn(1)	0.12893(8)	0.36237(7)	0	0.01140(15)
Cu(1)	0	0	0.24848(11)	0.01355(17)
O(1)	0.0776(5)	0.1350(4)	½	0.0114(8)
O(2)	0.1013(5)	0.1220(4)	0	0.0119(7)
O(3)	0.3944(5)	0.1054(4)	½	0.0177(8)
O(4)	0.2629(4)	0.3554(3)	0.2749(5)	0.0166(6)
H	0.191(9)	0.072(7)	0	0.018**

*Site occupancy: $M = Zn_{1.00}$

Table 4. Selected bond distances (Å) and angles (°) for austinite and zincolivenite from Tripi mine.

Austinite		Zincolivenite	
Ca–O(5)	2.309(3)	*Zn*(1)–O(4)	1.999(3)
Ca–O(4)	2.447(3)	*Zn*(1)–O(4)	1.999(3)
Ca–O(1)	2.502(3)	*Zn*(1)–O(3)	2.003(4)
Ca–O(2)	2.521(4)	*Zn*(1)–O(2)	2.064(4)
Ca–O(3)	2.538(3)	*Zn*(1)–O(3)	2.083(4)
Ca–O(2)	2.566(3)	<*Zn*–O>	2.030
Ca–O(3)	2.616(3)		
Ca–O(4)	2.657(3)		
<Ca–O>	2.520		
M–O(5)	1.936(3)	*Cu*(1)–O(1)	2.006(3)
M–O(5)	1.951(3)	*Cu*(1)–O(1)	2.006(3)
M–O(1)	2.085(3)	*Cu*(1)–O(2)	2.008(3)
M–O(4)	2.189(3)	*Cu*(1)–O(2)	2.008(3)
M–O(3)	2.212(3)	*Cu*(1)–O(4)	2.359(3)
M–O(1)	2.234(3)	*Cu*(1)–O(4)	2.359(3)
<*M*–O>	2.101	<*Cu*–O>	2.124
As–O(4)	1.681(3)	*As*(1)–O(4)	1.679(3)
As–O(2)	1.684(3)	*As*(1)–O(4)	1.679(3)
As–O(3)	1.689(3)	*As*(1)–O(3)	1.682(4)
As–O(1)	1.697(3)	*As*(1)–O(1)	1.694(4)
<*As*–O>	1.688	<*As*–O>	1.684
O(5)–H	0.85(3)	O(2)–H	0.87(3)
O(5)···O(2)	2.719(5)	O(2)···O(4)	2.883(4)
O(5)–H–O(2)	176(6)°	O(2)–H–O(4)	123(4)°

Zincolivenite

A total of 1368 frames was collected, with exposure time of 25 s per frame. Unit-cell parameters are $a = 8.4594(9)$, $b = 8.5324(8)$, $c = 5.9893(6)$ Å, $V = 432.30(12)$ Å^3 and space group *Pnnm*, in accord with systematic absences and the $|E^2-1|$ value (i.e. 0.861). The crystal structure was refined starting from the atomic coordinates given by Chukanov *et al.* (2007) for zincolivenite. The following scattering curves were used: As, Cu and Zn at the *As*(1), *Cu*(1) and *Zn*(1) sites, and O at the O(1)–O(4) sites. Owing to the similar scattering factors of Cu ($Z = 29$) and Zn ($Z = 30$), the site occupancy of the *Cu*(1) and *Zn*(1) sites was refined assuming a pure occupancy. After several cycles of isotropic refinement, the R_1 factor converged to 0.0520, confirming the correctness of the structural model. Introducing the anisotropic displacement parameters for all the atoms decreased the R_1 to 0.0234. The site hosting the H atom was not correctly located in the difference-Fourier maps and it was added on the basis of the atom coordinates given by Chukanov *et al.* (2007). A restraint on the O(2)–H bond distance was added and the displacement parameter of the H atom was restrained to be 1.5 times that of O(2). The refinement converged to $R_1 = 0.0230$ for 523 unique reflections with $F_o > 4\sigma(F_o)$ and 47 least-square parameters.

https://doi.org/10.1180/mgm.2023.49 Published online by Cambridge University Press

Table 5. Weighted bond-valence sums (in valence units) for austinite and zincolivenite from the Tripi mine.

Austinite Sites	*Ca*	*Zn*	*As*	Σ_{anions}	Σ_{anions}*	Theoretical
O(1)	0.23	0.35, 0.24	1.20	2.02	2.02	2.00
O(2)	0.22, 0.20		1.25	1.67	1.89	2.00
O(3)	0.21, 0.18	0.25	1.23	1.87	1.87	2.00
O(4)	0.27, 0.16	0.27	1.26	1.96	1.96	2.00
O(5)	0.38	0.52, 0.50		1.40	1.18	1.00
$\Sigma_{cations}$	1.85	2.13	4.94			
Theoretical	2.00	2.00	5.00			
Zincolivenite						
Sites	*Zn*(1)	*Cu*(1)	*As*(1)	Σ_{anions}	Σ_{anions}*	Theoretical
O(1)		$^{2\times\downarrow}0.41^{2\times\rightarrow}$	1.22	2.04	2.04	2.00
O(2)	0.37	$^{2\times\downarrow}0.41^{2\times\rightarrow}$		1.19	1.03	1.00
O(3)	0.43, 0.35		1.26	2.04	2.04	2.00
O(4)	$^{2\times\downarrow}$0.44	$^{2\times\downarrow}$0.16	$^{2\times\downarrow}$1.28	1.88	1.96	2.00
$\Sigma_{cations}$	2.03	1.96	5.04			
Theoretical	2.00	2.00	5.00			

Notes: left and right superscripts indicate the number of equivalent bonds involving anions and cations, respectively. The following site occupancies were used for calculating the bond-valence sums: in austinite, *Ca* = $Ca_{1.00}$, *Zn* = $Zn_{0.90}Cu_{0.10}$ and *As* = $As_{0.98}P_{0.02}$; in zincolivenite, *Cu*(1) = $Cu_{0.75}Zn_{0.25}$, *Zn*(1) = $Zn_{1.00}$ and *As*(1) = $As_{1.00}$.
* Corrected for H bonds.

Results and discussion

Chemical data

Chemical formulae of austinite, conichalcite and zincolivenite were recalculated on the basis of 3 cations per formula unit (pfu), assuming the presence of the amount of H_2O required to achieve the electrostatic balance.

The total of conichalcite is low, even after the addition of calculated H_2O; this is probably due to the small size of the polished grain embedded in epoxy. Such low totals were observed previously by other authors during the examination of this species (e.g. Braithwaite *et al.*, 2009). However, atom ratios agree with the ideal formula of this mineral.

Austinite and conichalcite and their solid-solution series

The chemical formula of austinite from the Tripi mine is $Ca_{1.04(1)}Zn_{0.86(4)}Cu_{0.09(4)}As_{0.98(2)}P_{0.02(1)}O_4(OH)_{0.98}$, whereas that of conichalcite is $Ca_{0.98(1)}Fe^{2+}_{0.02(4)}Cu_{0.69(10)}Zn_{0.30(6)}As_{0.97(2)}P_{0.03(1)}O_4(OH)_{0.98}$. With respect to the ideal formula, austinite has minor Cu-to-Zn and P-to-As substitutions, and a slight Ca excess; on the contrary, in conichalcite the replacement of Zn by Cu is significant. Minor Fe, assumed as Fe^{2+}, may partially replace Ca^{2+} or Zn^{2+}. However, owing to the oxidised nature of the assemblage studied, the occurrence of Fe^{3+} cannot be discarded. The relationship between the Zn and Cu contents, in atoms pfu, in austinite and conichalcite is shown in Fig. 2. Austinite has a Cu/(Cu + Zn) atomic ratio ranging between 0.03 and 0.23, whereas conichalcite from Tripi has the same ratio in the range 0.58–0.77.

Further analytical data from literature for the isotypic series between austinite and conichalcite analysis is also plotted in Fig. 2. Type material of the former was Cu free (Staples, 1935) and other occurrences of austinite are usually Cu poor. For instance, Giuseppetti and Tadini (1988) reported the replacement of Zn by 0.03 Cu atoms and 0.01 Fe atoms pfu for a sample from Kamareza (Greece), whereas Clark *et al.* (1997) gave the composition $Ca(Zn_{0.95}Cu_{0.03}Mg_{0.02})AsO_4(OH)$ for a sample from Sonora (Mexico). Gunter (1977) provided several analyses of members of the austinite–conichalcite series, with Cu/(Cu + Zn) atomic ratios in the range 0.47–1.00. Lead-bearing conichalcite described by

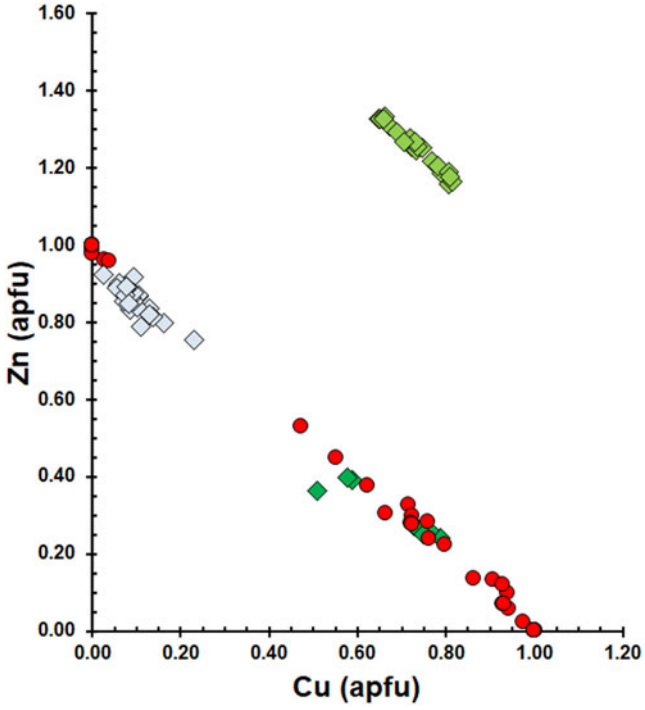

Figure 2. Relationship between Cu and Zn (in atoms per formula unit) in austinite (grey diamonds), conichalcite (green diamonds) and zincolivenite (light green diamonds) from the Tripi mine. Red circles indicate compositional data for austinite and conichalcite after Staples (1935), Radcliffe and Simmons (1971), Gunter (1977), Jambor *et al.* (1980), Giuseppetti and Tadini (1988), Henderson *et al.* (2008), Sakai *et al.* (2009) and Đorđević *et al.* (2016).

Jambor *et al.* (1980) has a Cu/(Cu + Zn) ratio in the interval 0.69–0.91, and similarly Taggart and Foord (1980), on the basis of electron dispersive spectroscopy data, found ratios of 0.11 for Cu-rich austinite and 0.60 for conichalcite. Henderson *et al.* (2008) refined a sample of conichalcite from the RRUFF project with only 0.01 Zn pfu. Other specimens of conichalcite from RRUFF have up to 0.30 Zn apfu (see http://rruff.info – Lafuente

https://doi.org/10.1180/mgm.2023.49 Published online by Cambridge University Press

et al., 2015). Conichalcite studied by Sakai *et al.* (2009) has no Zn, and Cu was partly replaced by very small amounts of Mg (up to 0.13 atoms pfu in a sample from Fukushima, Japan). Finally, conichalcite studied by Đorđević *et al.* (2016) has a Cu/(Cu + Zn) ratio of 0.97.

It is interesting to note that type material of the Pb-analogue of austinite, arsendescloizite $PbZn(AsO_4)(OH)$, contains no Cu (Keller and Dunn, 1982), whereas the P-analogue of conichalcite, hermannroseite, ideally $CaCu(PO_4)(OH)$, has a very small Zn content (Schlüter *et al.*, 2011).

Notwithstanding the hypothesis of Radcliffe and Simmons (1971) who suggested a complete solid solution between austinite and conichalcite, the evidence is meagre. Indeed, Fig. 2 suggests the possible existence of a miscibility gap in the compositional region having Cu/(Cu + Zn) in the range 0.25–0.50, i.e. $(Zn_{0.25}Cu_{0.75})$–$(Zn_{0.50}Cu_{0.50})$. This could be due to the Jahn-Teller effect shown by Cu^{2+} (Burns and Hawthorne, 1996); indeed, it is well-known that Cu^{2+} and Zn often tend to be partitioned in different structural sites, characterised by a different degree of distortion, e.g. in paratacamite and herbertsmithite (Braithwaite *et al.*, 2004), in rosasite (Perchiazzi, 2006), in ktenasite (Mellini and Merlino, 1978) and in zincolivenite (Chukanov *et al.*, 2007). The finding of both austinite and conichalcite in the same small vugs of a calcite vein from the Tripi mine is in keeping with this hypothesis; indeed, two distinct phases crystallised instead of a single phase with intermediate composition.

Zincolivenite

The chemical formula of zincolivenite from the Tripi mine is $Cu_{0.73(5)}Zn_{1.25(5)}As_{1.01(1)}O_4(OH)_{1.01}$. The Cu/(Cu + Zn) atomic ratio ranges between 0.33 and 0.41 (Fig. 2). This occurrence is richer in Zn than type material from the Lavrion deposit (Greece), having composition $Cu_{0.94}Zn_{1.03}Fe_{0.02}[(AsO_4)_{0.98}(PO_4)_{0.02}](OH)_{0.98}(H_2O)_{0.10}$, it is close to a sample from Dal′negorsk (Russia), with composition $Cu_{0.58}Mg_{0.07}Zn_{1.36}(AsO_4)(OH)_{0.98}O_{0.02}$ (Chukanov *et al.*, 2007). According to these authors, the chemical composition of zincolivenite should span the range between $Cu_{0.5}Zn_{1.5}(AsO_4)(OH)$ and $Cu_{1.5}Zn_{0.5}(AsO_4)(OH)$. Zinc-rich zincolivenite from the Tripi mine also has a composition similar to the specimen reported by Šejkora *et al.* (2008) from Krupka, northern Bohemia (Czech Republic), with composition $(Zn_{1.27}Cu_{0.62}Al_{0.08}Pb_{0.01}Ca_{0.01})[(AsO_4)_{0.98}(PO_4)_{0.01}(SO_4)_{0.01}](OH)_{1.09}$. Other quantitative data on zincolivenite are given by Gołębiowska *et al.* (2006), Braithwaite *et al.* (2009) and Andersen and Moulding (2009).

Micro-Raman spectroscopy

Austinite and conichalcite

The Raman spectra of austinite and conichalcite are shown in Fig. 3. The observed bands are at similar positions and only minor differences, in the lower wavenumber region, were observed.

In the region between 100 and 1200 cm^{-1}, the strongest Raman band occurs at 828 and 831 cm^{-1} for austinite and conichalcite, respectively, with two additional weaker bands at 784 and 805 cm^{-1} in both Raman spectra. These bands can be attributed to the ν_3 and ν_1 modes of AsO_4 groups, in agreement with Reddy *et al.* (2005) and Đorđević *et al.* (2016). It is worth noting that, in this spectral region, Martens *et al.* (2003b) also reported strong bands at 859 and 889 cm^{-1}. However these bands have not been observed in the sample from the Tripi mine or in isotypic phases like cobaltaustinite $CaCo(AsO_4)(OH)$ and nickelaustinite $CaNi(AsO_4)(OH)$. Finally, the occurrence of these bands do not agree with the infrared spectral features described by Sumin de Portilla (1974). In conclusion, the spectrum of austinite reported by Martens *et al.* (2003b) is not representative of this species. In the sample from the Tripi mine, two very weak bands occur at 920 and 975 cm^{-1} and at 924 and 975 cm^{-1} in the Raman spectra of austinite and conichalcite, respectively, and they could be attributed to the O–H deformation modes (e.g. Martens *et al.*, 2003b; Reddy *et al.*, 2005).

In the spectrum of austinite, bands at 381, 430 and 466 cm^{-1} can be related to the ν_4 bending modes of AsO_4 groups; these bands were observed at 394, 424 and 469 cm^{-1} in the spectrum of conichalcite. Weak bands at 502 cm^{-1} for austinite and at 502 and 518 cm^{-1} in conichalcite may be interpreted as due to ν_4 modes, although these band could be due to M–O stretching vibrations, in agreement with Martens *et al.* (2003b) who proposed such a possible interpretation for bands at 487 and 495 cm^{-1} observed in cobaltaustinite and nickelaustinite, respectively. The ν_2 bending modes of AsO_4 groups is possibly related to the bands at 328 and 347 cm^{-1} in the spectrum of austinite and at 330 and 353 cm^{-1} in that of conichalcite. Raman bands at lower wavenumbers, i.e., 134, 173, 216 and 281 cm^{-1} in austinite and 144, 188, 218 and 283 cm^{-1} in conichalcite, can be interpreted either as lattice modes or M–O vibrations.

In the region between 3000 and 4000 cm^{-1}, a relatively strong band at 3265 cm^{-1} was observed in both austinite and conichalcite, with a shoulder at 3330 cm^{-1}. These bands are related to the O–H stretching modes. Whereas in the olivenite–adamite series the band shift in the O–H stretching region can allow prediction of the local cation arrangements around the (OH) group (see below), this seems to be not applicable to the austinite–conichalcite isotypic pair. In these compounds, the (OH) group is bonded to one Ca and two *M* cations (*M* = Zn or Cu in austinite and conichalcite, respectively). It is worth noting that the *M*–(OH) bonds are the shortest ones in the M-centred octahedra; the replacement of Zn^{2+} by Cu^{2+}, the latter being responsible for the Jahn-Teller effect distorting the coordination polyhedron (Burns and Hawthorne, 1996), did not significantly affect such short distances. For this reason, the O···O distance of the H-bonds in austinite and conichalcite may be not so different to give rise to significant Raman shifts, i.e. 2.721–2.723 Å in austinite (Giuseppetti and Tadini, 1988; Clark *et al.*, 1997) and 2.741 Å in conichalcite (Sakai *et al.*, 2009). However, Henderson *et al.* (2008) reported a shorter O···O distance for conichalcite, i.e. 2.678 Å, stating that, in agreement with the relations between O···O and the wavenumber of O–H stretching modes (Libowitzky, 1999), conichalcite should show the smallest O–H wavenumber in the adelite series. In this respect, they cited the band at 3158 cm^{-1} observed by Martens *et al.* (2003b); a similar band position was reported by Reddy *et al.* (2005) at 3148 cm^{-1}. This band position corresponds, according to Libowitzky (1999), to an O···O distance of ca. 2.69 Å, in agreement with the distance observed by Henderson *et al.* (2008). This seems to suggest that a systematic study of the spectral features of the O–H stretching region on well-characterised specimens of the austinite–conichalcite isotypic series is mandatory to understand the actual relations between their crystal chemistry and band positions.

Zincolivenite

The Raman spectrum of zincolivenite is shown in Fig. 3. The region between 100 and 1200 cm^{-1} is characterised by two strong

https://doi.org/10.1180/mgm.2023.49 Published online by Cambridge University Press

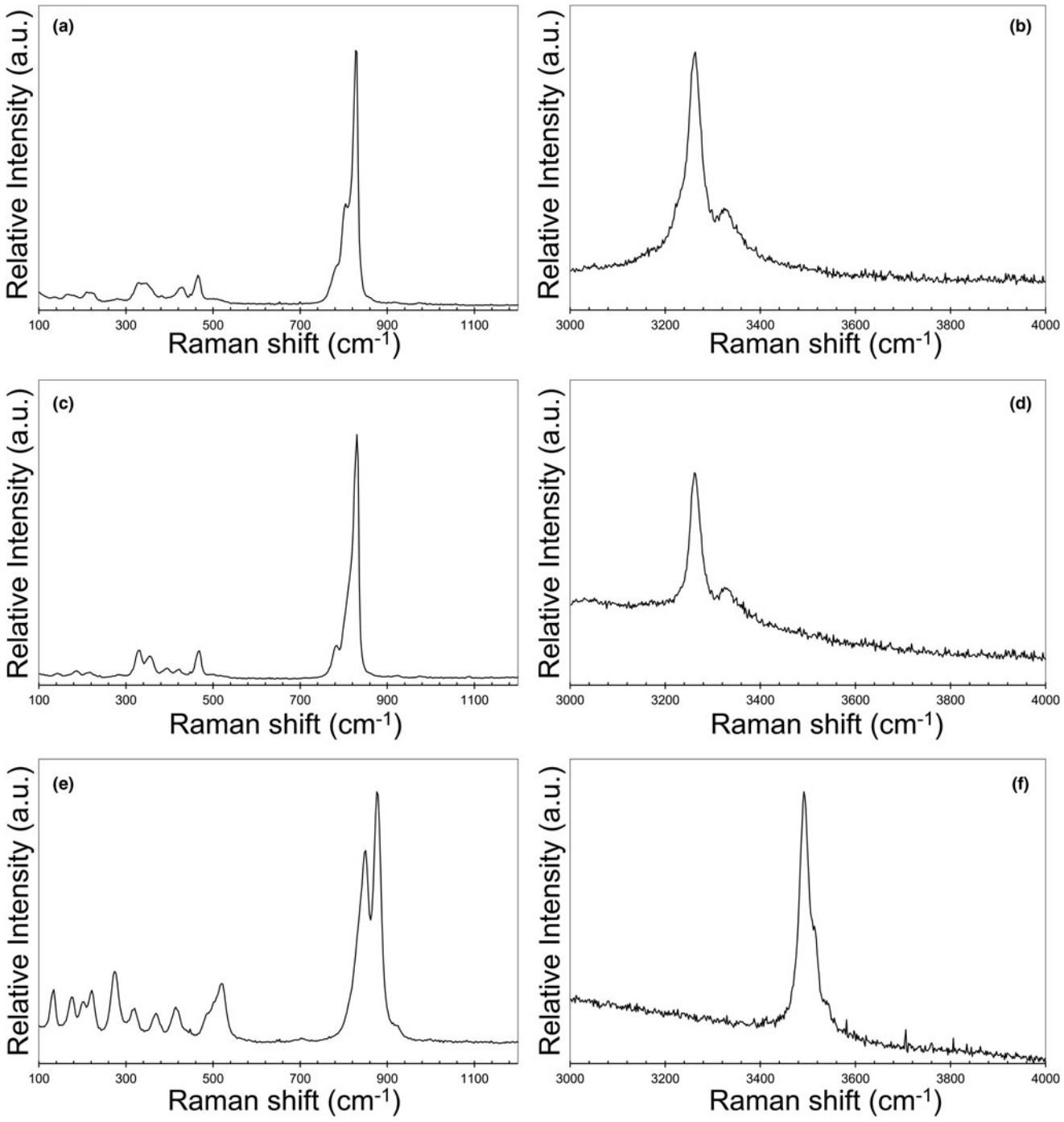

Figure 3. Raman spectra of austinite (a,b), conichalcite (c,d) and zincolivenite (e,f) in the region between 100–1200 cm^{-1} and 3000–4000 cm^{-1}.

bands at 850 and 876 cm^{-1}, with a weak shoulder at 924 cm^{-1}.The strong bands can be interpreted as due to the ν_3 and ν_1 stretching modes of AsO_4 groups, in agreement with Martens *et al.* (2003a) and Makreski *et al.* (2013). The weak shoulder at 924 cm^{-1} could be due to O–H deformation modes, as in the austinite–conichalcite pair (see above).

Bands at 487, 502 and 520 cm^{-1} can be interpreted as due to the ν_4 bending modes of AsO_4 groups, whereas the ν_2 modes can be represented by the band at 414 cm^{-1}. Makreski *et al.* (2013) interpreted the bands at 325 and 380 cm^{-1} in the Raman spectrum of adamite as due to the vibrations of $M^{2+}O_5$ unit; in agreement with this interpretation, a similar attribution can be proposed for the bands at 320 and 369 cm^{-1} observed in zincolivenite from the Tripi mine. Finally, bands at 135, 175, 202, 222 and 274 cm^{-1} are probably due to M–O modes and lattice vibrations.

In the 3000–4000 cm^{-1} region, three sharp bands were observed at 3492, 3514 and 3540 cm^{-1}. These three bands can be interpreted as due to O–H stretching modes and they can be related to different local Cu–Zn distributions, in agreement with the interpretation of Chisholm (1985), based on previous results of Braithwaite (1983). Taking into account the electron

https://doi.org/10.1180/mgm.2023.49 Published online by Cambridge University Press

microprobe data of zincolivenite from the Tripi mine, the site occupancy ($Cu_{0.75}Zn_{0.25}$) and $Zn_{1.00}$ can be proposed for the *Cu*(1) and *Zn*(1) sites, respectively. As the (OH) group is bonded to one *Zn*(1) and two *Cu*(1) sites, the following cation distributions around the (OH) group can be observed [elements are listed according to the occupancy of sites *Zn*(1)*Cu*(1)*Cu*(1)]: (i) ZnCuCu; (ii) ZnCuZn; and (iii) ZnZnZn. In agreement with Chisholm (1985), these three different local arrangements should correspond to bands at 3490, 3510 and 3540 cm^{-1}, comparable with the values observed in the Sicilian sample studied in this work. Moreover, considering the relative proportions of Zn and Cu, configuration (i) is more abundant than configurations (ii) and (iii). Through the fitting of the O–H stretching bands using *Fityk* (Wojdyr, 2010), a ratio 75:17:8 for the three possible arrangements has been obtained. This ratio can be taken into account qualitatively to indicate that ZnCuCu is the most probable configuration, followed by the configurations ZnCuZn and ZnZnZn, in agreement with the electron microprobe data and the Cu and Zn preferential partitioning at *Cu*(1) and *Zn*(1) sites, respectively.

Crystal structure description

Austinite and conichalcite

Austinite and conichalcite belong to the adelite group within the descloizite supergroup. In agreement with previous authors (Qurashi and Barnes, 1963; Giuseppetti and Tadini, 1988; Clark *et al.*, 1997; Henderson *et al.*, 2008; Sakai *et al.*, 2009; Đorđević *et al.*, 2016), their crystal structure can be described as formed by columns of edge-sharing *M*-centred octahedra running along **c**; every chain is connected to four adjacent octahedral chains through corner-sharing As-centred tetrahedra. In the cavities resulting from this heteropolyhedral framework, eight-fold coordinated Ca^{2+} cations are hosted (Fig. 4). Following Eby and Hawthorne (1993), the structure of the isotypic pair austinite–conichalcite could be described as a $M = M–T$ framework, i.e. edge-sharing octahedral chains linked by tetrahedral corners.

In austinite, *M* is zinc. This element is octahedrally coordinated by four O^{2-} and two $(OH)^{-}$ groups. Bond distances range between 1.936 and 2.234 Å, with average <Zn–O> distance of 2.101 Å, to be compared with 2.104 and 2.106 Å observed by Giuseppetti and Tadini (1988) and Clark *et al.* (1997), respectively. The two shortest Zn–O distances are formed with (OH) groups (1.936 and 1.951 Å, respectively), in agreement with previous studies (Giuseppetti and Tadini, 1988; Clark *et al.*, 1997). The difference between the longest and shortest Zn–O distance is 0.297 Å, to be compared with 0.311 and 0.300 Å given by Giuseppetti and Tadini (1988) and Clark *et al.* (1997); this difference is increased in conichalcite, e.g. 0.476, 0.470 and 0.503–0.504 Å for conichalcite from Arizona, Japan and Chile, respectively (Henderson *et al.*, 2008; Sakai *et al.*, 2009; Đorđević *et al.*, 2016). This is due to the Jahn-Teller effect shown by Cu^{2+} (Burns and Hawthorne, 1996). Along the columns, Zn–Zn distance is 2.967 Å, close to 2.970 Å reported for the sample from Kamareza studied by Giuseppetti and Tadini (1988), whereas it is shorter than that observed by Clark *et al.* (1997) for the sample from Sonora, i.e. 2.977 Å. This is probably due to the minor replacement of Zn by Cu observed in the sample from Tripi. In conichalcite, indeed, the Cu–Cu distance along the **c** direction is 2.92–2.93 Å (Qurashi and Barnes, 1963; Sakai *et al.*, 2009). According to Clark *et al.* (1997), the value observed by Giuseppetti and Tadini (1988) could indicate some Cu substitution, in agreement with data of austinite from the Tripi mine. The bond-valence sum at the *Zn* site, calculated assuming the site population ($Zn_{0.90}Cu_{0.10}$), is 2.11 valence units (vu) (Table 5).

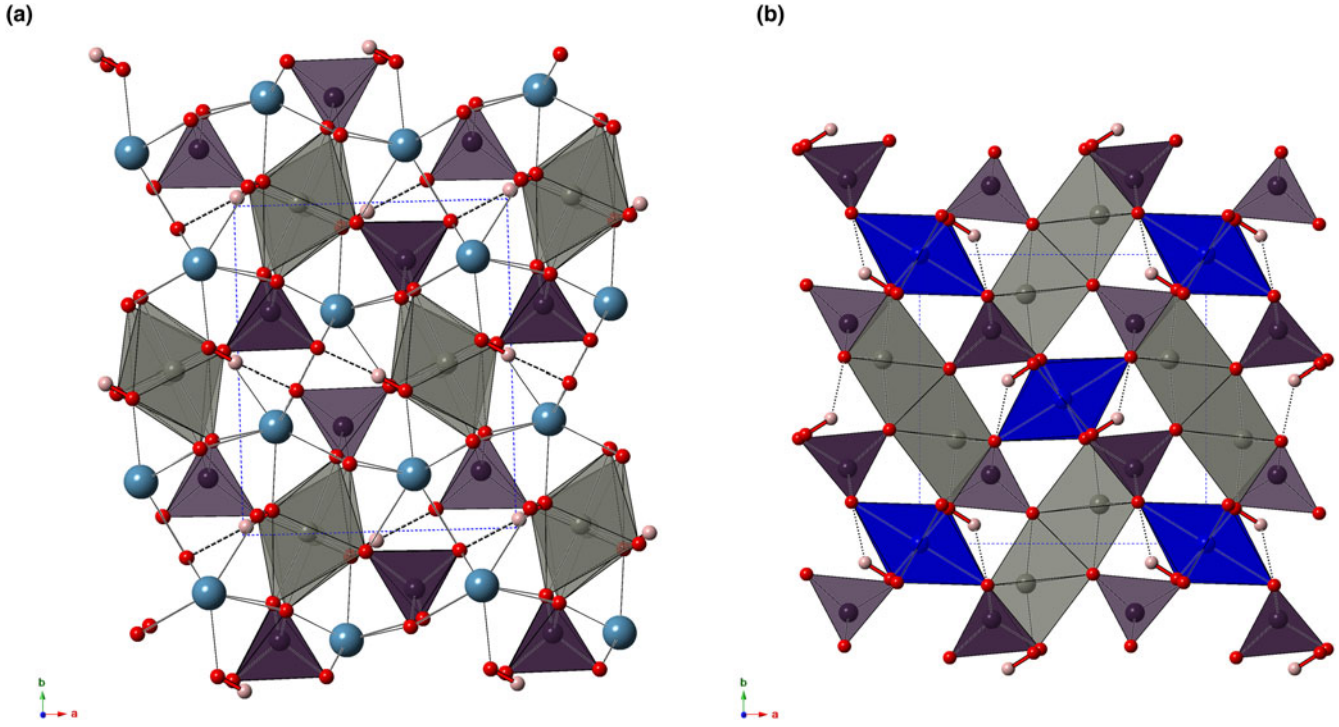

Figure 4. Crystal structures of austinite (a) and zincolivenite (b) seen down **c**. Arsenic-, Cu- and Zn-centred polyhedra are shown in violet, blue and grey, respectively. Circles represent Ca (light blue), O (red) and H (pink) atoms. Thick red lines and dashed black lines are, respectively, O–H and H···O bonds. Unit cells are shown as blue dotted lines. Drawn with *CrystalMaker®* software.

https://doi.org/10.1180/mgm.2023.49 Published online by Cambridge University Press

Arsenic is tetrahedrally coordinated, with As–O bonds ranging between 1.681 and 1.697 Å. The average <As–O> bond distance is 1.688 Å, comparable to 1.692 and 1.694 Å of Giuseppetti and Tadini (1988) and Clark *et al.* (1997), respectively, and fitting with the grand value of 1.688 Å given by Majzlan *et al.* (2014). The bond-valence sum at this site, calculated with the site occupancy ($As_{0.98}P_{0.02}$), is 4.94 vu (Table 5), in agreement with the occurrence of As^{5+}.

Calcium is coordinated by seven O^{2-} and one $(OH)^{-}$ group in a distorted square antiprism. Calcium–O distances range between 2.309 and 2.657 Å, the shortest distance being represented by the Ca–(OH) bond. These distances can be compared with the results of Giuseppetti and Tadini (1988) and Clark *et al.* (1997), who reported Ca–O distances in the range 2.315–2.656 Å and 2.313–2.661 Å, respectively. The $CaO_7(OH)$ polyhedron shares edges with two AsO_4 tetrahedra and three edges with Zn-centred octahedra; the edges shared with AsO_4 groups are the shortest ones in the Ca-centred polyhedron. The bond-valence sum at the *Ca* site is 1.85 vu (Table 5).

Oxygen atoms are three- or four-fold coordinated by Ca, Zn and As atoms. Those atoms hosted at O(1), O(2) and O(4) sites are bonded to these three cations, achieving bond-valence sums ranging between 1.87 and 2.02 vu, in agreement with the occurrence of O^{2-} anions. On the contrary, oxygen atoms at O(2) and O(5) are three-fold coordinated. The former is bonded to two Ca and one As atom, with a bond-valence sum of 1.67 vu, whereas the latter is bonded to one Ca and two Zn atoms, with a bond-valence sum of 1.40 vu. The undersaturation of O(2) and O(5) indicates their involvement in the O(5)–H···O(2) hydrogen bond. The O(5)···O(2) distance is 2.719(5) Å, to be compared with 2.721 and 2.723 Å given by Giuseppetti and Tadini (1988) and Clark *et al.* (1997); using relationships between bond distance and bond strength in H bonds from Ferraris and Ivaldi (1988), such a distance corresponds to a bond strength of 0.22 vu. These values agree with the O···O distances estimated on the basis of the wavenumbers of O–H stretching modes observed in the Raman spectrum of austinite following Libowitzky (1999), i.e. 2.726 and 2.755 Å, respectively.

Zincolivenite

Zincolivenite belongs to the olivenite group, a series of orthorhombic and monoclinic arsenates and phosphates whose crystal structures are related to that of andalusite, Al_2SiO_4O. The crystal structure of zincolivenite can be described as formed by chains of edge-sharing distorted $Cu(1)O_4(OH)_2$ octahedra running along **c**. These octahedral chains are connected by isolated $As(1)O_4$ tetrahedra through corner-sharing, giving rise to channels where dimers of edge-sharing $Zn(1)O_4(OH)$ trigonal bipyramids are hosted.

Copper is in a distorted octahedral coordination. Bond distances range between 2.006 and 2.359 Å, with an average value of 2.124 Å. These values can be compared with those given by Chukanov *et al.* (2007) for type zincolivenite from Lavrion, Greece and by Toman (1978) for a sample from Tsumeb, Namibia. The former has an average <Cu–O> distance of 2.132 Å (range 1.986–2.409 Å) and the latter 2.12 Å (range 1.99–2.37 Å). It is interesting to observe that the difference between the longest and shortest Cu–O distances is 0.35, 0.38 and 0.42 Å for the samples from Tripi, Tsumeb, and Lavrion, respectively; this increasing difference is directly related to the Cu content. Indeed, the Cu/(Cu + Zn) atomic ratios of these three studied samples are 0.37, 0.42 and 0.48, respectively. The higher the Cu content, the higher is the distortion of the Cu-centred Cu(1) octahedron. This is in keeping with the Jahn-Teller effect shown by Cu^{2+} (Burns and Hawthorne, 1996). In the Tripi mine, the *Cu*(1) site is probably a mixed (Cu,Zn) site, with an idealised site occupancy ($Cu_{0.75}Zn_{0.25}$), based on electron microprobe data. The bond-valence sum at this site, calculated using this site occupancy, is 1.96 vu. (Table 5).

Zinc is hosted at the *Zn*(1) site. In zincolivenite from the Tripi mine, the average <Zn–O> is 2.030 Å, with bond distances ranging between 1.999 and 2.083 Å. These features are close to those observed in the Greek and Namibian specimens by Chukanov *et al.* (2007) and Tomin (1978), respectively. In the former, the average distance is 2.031 Å (range 1.998–2.074 Å), and in the latter 2.04 Å (range 2.00–2.08 Å). The bond-valence sum at the *Zn*(1) site is 2.03 vu. (Table 5).

Arsenic is tetrahedrally coordinated, with As–O bonds ranging between 1.679 and 1.694 Å. Average <As–O> bond distance is 1.684 Å, comparable to 1.690 and 1.689 Å of Chukanov *et al.* (2007) and Tomin (1978). The bond-valence sum is 5.04 vu. (Table 5).

Among the four symmetry-independent O atoms, three have bond-valence sums ranging between 1.88 and 2.04 vu, whereas the fourth, namely the oxygen atom at the O(2) site, shows a strong undersaturation, i.e. 1.19 vu. This latter atom is involved in a H bond with O(4), with the O(2)–H···O(4) distance of 2.883(4) Å, corresponding to a bond strength of 0.16 vu. (according to Ferraris and Ivaldi, 1988); taking into account the bifurcated nature of this H bond (as, for instance, in adamite or the related phosphate libethenite – e.g. Cordsen, 1978; Jinnouchi *et al.*, 2016), the bond valence at the O(4) site is increased by 0.08 vu, up to 1.96 vu, in agreement with the occurrence of O^{2-} anions. The observed O···O distance agrees with the bond lengths calculated using the relation of Libowitzky (1999), i.e. between 2.88 and 2.97 Å.

Conclusions

The crystal chemical characterisation of austinite, conichalcite and zincolivenite is a further step in the knowledge of the supergene phases formed through the alteration of base-metal ore deposits of the Peloritani Mountains, after the study on the alunite-supergroup mineral kintoreite (Mauro *et al.*, 2022). In particular, the identification of these three arsenates gives interesting insights for the speciation, transport and dispersion of As in this sector of Sicily, where, as discussed briefly in the Introduction, high contents of this toxic element (as well as other PTE) have been reported in stream sediments and soils since the beginning of the 1990s (e.g. De Vivo *et al.*, 1993; Cosenza *et al.*, 2015).

This study also provides some interesting crystal-chemical and physical data for the arsenates studied. Some unexpected spectral features described by Martens *et al.* (2003b) in the Raman spectrum of austinite (i.e. the occurrence of strong bands at 889 and 859 cm^{-1}) are not supported by the current study, where the same grain used for single-crystal X-ray diffraction study and electron microprobe analysis was used for the collection of micro-Raman spectra. Some discrepancies occur also in the O–H stretching region, suggesting the opportunity to perform a systematic study on well-characterised specimens of the austinite–conichalcite isotypic series to describe the actual relations between crystal-chemistry and the band position of the O–H stretching modes. Moreover, a critical examination of the austinite–conichalcite isotypic pair suggests the existence of a miscibility gap between these two species, in

https://doi.org/10.1180/mgm.2023.49 Published online by Cambridge University Press

disagreement with the hypothesis of Radcliffe and Simmons (1971). This gap would not be surprising, considering the Jahn-Teller effect shown by Cu^{2+} cations and the Zn/Cu different partitioning observed in several mineral species. One of them is represented by zincolivenite. The refinement of the crystal structure of Zn-rich zincolivenite from the Tripi mine, with a Cu/(Cu + Zn) atomic ratio different from the samples studied previously by Toman (1978) and Chukanov *et al.* (2007), has shown that, between *Cu*(1) and *Zn*(1), only the former seems to be affected by geometrical changes related to the different chemistry. Majzlan *et al.* (2023) stated that anomalous X-ray diffraction would be required to prove cation ordering in zincolivenite. This is correct, but it should be noted that examination of the geometrical features of the *Cu*(1) and *Zn*(1) sites in the available refinements of zincolivenite supports the presence of Cu and Zn ordering; the study of other specimens, possibly Cu-rich, may be able to support or refute this statement.

Acknowledgements. Peter Leverett and an anonymous reviewer are acknowledged for their useful comments. R. Gunter is thanked for making available his B.Sc. Thesis. This research was financially supported by the Ministero dell'Istruzione, Università e Ricerca through the project PRIN 2017 "TEOREM – deciphering geological processes using Terrestrial and Extraterrestrial ORE Minerals", prot. 2017AK8C32 and by the Ministry of Culture of the Czech Republic (long-term project DKRVO 2019–2023/1.II.e; National Museum, 00023272) for JS.

Supplementary material. The supplementary material for this article can be found at https://doi.org/10.1180/mgm.2023.49.

Competing interests. The authors declare none.

References

Andersen J.C.Ø. and Moulding D. (2009) Zincolivenite from the Penberthy Croft mine, Cornwall. *Journal of the Russell Society*, **12**, 10–14.

Braithwaite R.S.W. (1983) Infrared spectroscopic analysis of the olivenite–adamite series, and of phosphate substitution in olivenite. *Mineralogical Magazine*, **47**, 51–57.

Braithwaite R.S.W., Mereiter K., Paar W.H. and Clark A.M. (2004) Herbertsmithite, $Cu_3Zn(OH)_6Cl_2$, a new species, and the definition of paratacamite. *Mineralogical Magazine*, **68**, 527–539.

Braithwaite R.S.W., Green D.I. and Tindle A.G. (2009) The distribution and composition of adamite and zincolivenite in Britain and Ireland. *Journal of the Russell Society*, **12**, 3–9.

Bruker AXS Inc. (2022) *APEX4*. Bruker Advanced X-ray Solutions, Madison, Wisconsin, USA.

Burns P.C. and Hawthorne F.C. (1996) Static and dynamic Jahn-Teller effects in Cu^{2+} oxysalt minerals. *The Canadian Mineralogist*, **34**, 1089–1105.

Cangemi M., Censi V., Madonia P. and Favara R. (2021) Application of geostatistical tools to the geochemical characterization of the Peloritani Mts (Sicily, Italy) aquifers. *Water*, **2021**, 13.

Chisholm J.E. (1985) Cation segregation and the O–H stretching vibration of the olivenite-adamite series. *Physics and Chemistry of Minerals*, **12**, 185–190.

Chukanov N.V., Pushcharovsky D.Yu., Zubkova N.V., Pekov I.V., Pasero M., Merlino S., Möckel S., Rabadanov M.Kh. and Belakovskiy D.I. (2007) Zincolivenite $CuZn(AsO_4)(OH)$: a new adamite-group mineral with ordered distribution of Cu and Zn. *Doklady Earth Sciences*, **415A**, 841–845.

Clark L.A., Pluth J.J., Steele I., Smith J.V. and Sutton S.R. (1997) Crystal structure of austinite, $CaZn(AsO_4)OH$. *Mineralogical Magazine*, **61**, 677–683.

Cordsen A. (1978) A crystal structure refinement of libethenite. *The Canadian Mineralogist*, **16**, 153–157.

Cosenza A., Lima A., Ayuso R.A., Foley N.K., Albanese S., Messina A. and De Vivo B. (2015) Soil geochemical survey of abandoned mining sites in the Eastern-Central Peloritani Mountains, Sicily, Italy. *Geochemistry: Exploration, Environment, Analysis*, **15**, 361–372.

Craw D. and Bowell R.J. (2014) The characterization of arsenic in mine waste. Pp. 473–505 in: *Arsenic: Environmental Geochemistry, Mineralogy, and Microbiology* (R.J. Bowell, C.N. Alpers, H.E. Jamieson, D.K. Nordstrom and J. Majzlan, editors). Reviews in Mineralogy and Geochemistry, **79**. The Mineralogical Society of America and the Geochemical Society, Chantilly, Virginia, USA.

De Vivo B., Lima A., Catalano G. and Chersicla A. (1993) Detailed geochemical survey in the Peloritani Arc (northeastern Sicily, Italy): Evidence of gold anomalies. *Journal of Geochemical Exploration*, **46**, 309–324.

Donati G., Stagno F. and Triscari M. (1978) Ricerche sulle mineralizzazioni metallifere dei M. Peloritani. III) Giacimenti delle C.de S. Carlo, Montagne e viciniori presso Fiumedinisi (Messina). *Atti dell'Accademia Peloritana dei Pericolanti, Classe di Scienze Matematiche, Fisiche e Naturali*, **56**, 177–238.

Dongarrà G., Manno E., Sabatino G. and Varrica D. (2009) Geochemical characteristics of waters in mineralised area of Peloritani Mountains (Sicily, Italy). *Applied Geochemistry*, **24**, 900–914.

Đorđević T., Kolitsch U. and Nasadala L. (2016) A single-crystal X-ray and Raman spectroscopic study of hydrothermally synthesized arsenates and vanadates with the descloizite and adelite structure types. *American Mineralogist*, **101**, 1135–1149.

Drahota P. and Filippi M. (2009) Secondary arsenic minerals in the environment: A review. *Environment International*, **35**, 1243–1255.

Eby R.K. and Hawthorne F.C. (1993) Structural relations in copper oxysalt minerals. I. Structural hierarchy. *Acta Crystallographica*, **B49**, 28–56.

Ferraris G. and Ivaldi G. (1988) Bond valence vs bond length in O···O hydrogen bonds. *Acta Crystallographica*, **B44**, 341–344.

Flack H.D. (1983) On enantiomorph-polarity estimation. *Acta Crystallographica*, **A39**, 876–881.

Gagné O.C. and Hawthorne F.C. (2015) Comprehensive derivation of bond-valence parameters for ion pairs involving oxygen. *Acta Crystallographica*, **B71**, 562–578.

Gieré R., Sidenko N.V. and Lazareva E.V. (2003) The role of secondary minerals in controlling the migration of arsenic and metals from high-sulfide wastes (Berikul gold mine, Siberia). *Applied Geochemistry*, **18**, 1347–1359.

Giuseppetti G. and Tadini C. (1988) The crystal structure of austinite, $CaZn(AsO_4)(OH)$, from Kamareza, Laurion (Greece). *Neues Jahrbuch für Mineralogie, Monatshefte*, **1988**, 159–166.

Gołębiowska B., Pieczka A. and Franus W. (2006) Olivenite-adamite solid solution from oxidation zone in Rędziny (West Sudetes, Poland). *Mineralogia Polonica*, **37**, 97–107.

Gunter R. (1977) *Conichalcite–Austinite Solid Solution Series*. B.Sc. Thesis, Queen's University, Kingston, Ontario, Canada, 28 p.

Henderson R.R., Yang H., Downs R.T. and Jenkins R.A. (2008) Redetermination of conichalcite, $CaCu(AsO_4)(OH)$. *Acta Crystallographica*, **E64**, i53–i54.

Jambor J.L., Owens D.R. and Dutrizac J.E. (1980) Solid solution in the adelite group of arsenates. *The Canadian Mineralogist*, **18**, 191–195.

Jinnouchi S., Yoshiasa A., Sugiyama K., Shimura R., Arima H., Momma K. and Miyawaki R. (2016) Crystal structure refinements of legrandite, adamite, and paradamite: The complex structure and characteristic hydrogen bonding network of legrandite. *Journal of Mineralogical and Petrological Sciences*, **111**, 35–43.

Keller P. and Dunn P.J. (1982) Arsendescloizite a new mineral from Tsumeb. *The Mineralogical Record*, **13**, 155–157.

Lafuente B., Downs R.T., Yang H. and Stone N. (2015) The power of databases: the RRUFF project. Pp. 1–30 in: *Highlights in Mineralogical Crystallography* (T. Armbruster and R.M. Danisi, editors). De Gruyter, Berlin, Germany.

La Valle G. (1898) Su di alcuni nuovi minerali cobaltiferi e nichiliferi nella provincia di Messina. *Atti della R. Accademia dei Lincei, Rendiconti*, **7**, 68–71.

Libowitzky E. (1999) Correlation of O–H stretching frequencies and O–H···O hydrogen bond lengths in minerals. *Monatshefte für Chemie*, **130**, 1047–1059.

Majzlan J., Drahota P. and Filippi M. (2014) Parageneses and crystal chemistry of arsenic minerals. Pp.17–184 in: *Arsenic: Environmental Geochemistry, Mineralogy, and Microbiology* (R.J. Bowell, C.N. Alpers, H.E. Jamieson, D.K. Nordstrom and J. Majzlan, editors). Reviews in Mineralogy and Geochemistry, 79. The Mineralogical Society of America and the Geochemical Society, Chantilly, Virginia, USA.

Majzlan J., Števko M., Plášil J., Sejkora J. and Dachs E. (2023) Thermodynamics of the Cu, Zn, and Cu-Zn phases: zincolivenite, adamite, olivenite, ludjibaite, strashimirite, and slavkovite. *Journal of Geosciences*, **68**, 67–80.

Makreski P., Jovanovski S., Pejov L., Kloess G., Hoebler H.-J. and Jovanovski G. (2013) Theoretical and experimental study of the vibrational spectra of sarkinite $Mn_2(AsO_4)(OH)$ and adamite $Zn_2(AsO_4)(OH)$. *Spectrochimica Acta*, **A113**, 37–42.

Martens W., Frost R.L., Kloprogge J.T. and Williams P.A. (2003a) The basic copper arsenate minerals olivenite, cornubite, cornwallite, and clinoclase: An infrared emission and Raman spectroscopic study. *American Mineralogist*, **88**, 501–508.

Martens W., Frost R.L. and Williams P.A. (2003b) Molecular structure of the adelite group of minerals – a Raman spectroscopic study. *Journal of Raman Spectroscopy*, **34**, 104–111.

Mauro D., Biagioni C. and Zaccarini F. (2021) New data on gersdorffite and associated minerals from the Peloritani Mountais (Sicily, Italy). *European Journal of Mineralogy*, **33**, 717–726.

Mauro D., Biagioni C. and Zaccarini F. (2022) A contribution to the mineralogy of Sicily, Italy – Kintoreite from the Tripi mine, Peloritani Mountains: occurrence and crystal structure. *Mineralogical Magazine*, **86**, 548–556.

Mellini M. and Merlino S. (1978) Ktenasite, another mineral with $^{2}_{\infty}[(Cu,Zn)_2(OH)_3O]^{-}$ octahedral sheets. *Zeitschrift für Kristallographie*, **147**, 129–140.

Mitchell V.L. (2014) Health risks associated with chronic exposures to arsenic in the environment. Pp. 435–449 in: *Arsenic: Environmental Geochemistry, Mineralogy, and Microbiology* (R.J. Bowell, C.N. Alpers, H.E. Jamieson, D.K. Nordstrom and J. Majzlan, editors). Reviews in Mineralogy and Geochemistry, **79**. The Mineralogical Society of America and the Geochemical Society, Chantilly, Virginia, USA.

Perchiazzi N. (2006) Crystal structure determination and Rietveld refinement of rosasite and mcguinnessite. *Zeitschrift für Kristallographie*, **23**, 505–510.

Pouchou J.L. and Pichoir F. (1985) "PAP" (φρZ) procedure for improved quantitative microanalysis. Pp. 104–106 in: *Microbeam Analysis* (J.T. Armstrong, editor). San Francisco Press, San Francisco.

Qurashi M.M. and Barnes W.H. (1963) The structures of the minerals of the descloizite and adelite groups: IV – Descloizite and conichalcite (Part 2). The structure of conichalcite. *The Canadian Mineralogist*, **7**, 561–577.

Radcliffe D. and Simmons W.B. (1971) Austinite: chemical and physical properties in relation to conichalcite. *American Mineralogist*, **56**, 1359–1365.

Reddy B.J., Frost R.L. and Martens W.N. (2005) Characterization of conichalcite by SEM, FTIR, Raman and electron reflectance spectroscopy. *Mineralogical Magazine*, **69**, 155–172.

Saccà C., Saccà D., Nucera P., De Fazio A. and D'Urso D. (2007) Geochemical and mineralogical features of the polymetallic deposit from Alì (NE Sicily, Italy). *Atti dell'Accademia Peloritana dei Pericolanti*, **85**, 1–12.

Saccà C., Saccà D. and Nucera P. (2015) *Le mineralizzazioni dei Monti Peloritani. Storia e attualità*. Aracne Editrice, Roma, 300 pp.

Sakai S., Yoshiasa A., Sugiyama K. and Miyawaki R. (2009) Crystal structure and chemistry of conichalcite, $CaCu(AsO_4)(OH)$. *Journal of Mineralogical and Petrological Sciences*, **104**, 125–131.

Schlüter J., Pohl D. and Gebhard G. (2011) The new mineral hermannroseite, $CaCu(PO_4,AsO_4)(OH)$, the phosphate analogue of conichalcite, from Tsumeb, Namibia. *Neues Jahrbuch für Mineralogie, Abhandlungen*, **188**, 135–140.

Sejkora J., Škovíra J. and Škoda R. (2008) Zincolivenite from the ore district Krupka, the Krušné hory Mts., Czech Republic). *Bulletin mineralogicko–petrologického oddělení Národního muzea v Praze*, **16**, 24–29 [in Czech].

Sheldrick G.M. (2015) Crystal structure refinement with SHELXL. *Acta Crystallographica*, **C71**, 3–8.

Staples L.W. (1935) Austinite, a new arsenate mineral, from Gold Hill, Utah. *American Mineralogist*, **20**, 112–119.

Sumin de Portilla V.I. (1974) Infrared spectroscopic investigation of the structure of some natural arsenates and the nature of H-bonds in their structures. *The Canadian Mineralogist*, **12**, 262–268.

Taggart J.E. Jr. and Foord E.E. (1980) Conichalcite, cuprian austinite, and plumbian conichalcite from La Plata County, Colorado. *The Mineralogical Record*, **11**, 37–38.

Toman K. (1978) Ordering in olivenite-adamite solid solutions. *Acta Crystallographica*, **B34**, 715–721.

Triscari M. (1985) A first occurrence of gersdorffite in the Peloritani Mts. (Sicily N.E.). *Rendiconti della Società Italiana di Mineralogia e Petrologia*, **40**, 289–294.

Triscari M. and Saccà C. (1982) Scheelite at the S. Carlo Sb-Cu-Ag mine, Fiumedinisi, Messina, Italy. *Mineralogica et Petrographica Acta*, **26**, 159–168.

Triscari M. and Saccà C. (1984) Contributo alla conoscenza dei minerali metalliferi dei Monti Peloritani (Sicilia N.E.) VI) La boulangerite. *Rendiconti della Società Italiana di Mineralogia e Petrologia*, **39**, 145–154.

Wilson A.J.C. (1992) *International Tables for Crystallography. Volume C: Mathematical, Physical and Chemical Tables*. Kluwer Academic Publishers, Dordrecht, The Netherlands.

Wojdyr M. (2010) Fityk: a general-purpose peak fitting program. *Journal of Applied Crystallography*, **43**, 1126–1128.

https://doi.org/10.1180/mgm.2023.49 Published online by Cambridge University Press